Theoret. Appl. Mech., Vol.38, No.4, pp. 299–319, Belgrade 2011

Experimental verification of stress-wave bands and negative phase velocity in layered media

Alireza V. Amirkhizi* **Sia Nemat-Nasser †**

Abstract

Based on a robust numerical method for calculation of band structure for stress-waves in heterogeneous media, a layered composite was designed and fabricated. It is shown that in the second pass band of this simple 2-phase layered structure, the direction of the energy flow is opposite that of the phase velocity. The ultrasonic stress-wave transmission through multiple thicknesses of this structure was studied experimentally and various quantities, such as band structure, phase velocity, group velocity, and a representation of the velocity of energy propagation were measured and compared with numerical predictions. The numerical calculations are based on hybrid (mixed min-max) variational principles presented previously by Nemat-Nasser and coworkers. In the cases where a closed form solution exists, the numerical results of this method agree very accurately with the results of the exact solution. Furthermore, the computational efficiency of the mixed variational method renders it an excellent tool for design and analysis of stress-wave propagation in heterogeneous media.

Keywords:layered media; periodic media; band structure; group velocity; phase velocity; negative refraction

1 Introduction

Propagation of waves in heterogeneous media with periodic microstructure has been studied extensively in the scientific literature [1, 2]. The shared attribute of all linear waves is the hyperbolic nature of the governing partial differential equations. Therefore, similar and equivalent techniques are

*Center of Excellence for Advanced Materials, University of California, San Diego, 0416, 9500 Gilman Drive, La Jolla, CA 92093-0416, e-mail: alireza@ucsd.edu

†Center of Excellence for Advanced Materials, University of California, San Diego, 0416, 9500 Gilman Drive, La Jolla, CA 92093-0416

used across disciplines. This congruence has been explicitly demonstrated, especially through introduction of similar variational principles [3, 4]

Pendry and coworkers analysis [5, 6] and the following experimental and numerical work by Smith and coworkers [7, 8] have spurred intense research on electromagnetic metamaterials, i.e. heterogeneous media for which (1) one may define overall (equivalent and homogenized) material properties and (2) such overall properties do not exist in naturally occurring materials. In almost all cases these media consist of a periodic arrangement of scattering elements. The overall response of the medium is affected by the geometry and properties of these scattering elements, especially when their resonance frequency is within the range of the frequency of the imposed waves. An interesting possibility discussed by these researchers was a medium with simultaneously negative overall effective electric permittivity and magnetic permeability. Veselago [9] studied the theoretical implications of the existence of materials with such overall properties and discussed a number of possible phenomena such as negative refraction of waves, i.e. anti-parallel group and phase velocities, and consequently, the reversal of Snell's law. The first experimental demonstration of such behavior was performed by Shelby et al. [10] We note that, on the pass band with anti-parallel group and phase velocities, the overall material response will be highly dissipative, even if the constituent components are only minimally dissipative.

There have been some efforts to reproduce such behavior in mechanical and acoustic waves (e.g [11, 12]). These works have mainly been focused on creating devices that would replicate the capacitative and inductive nature of the scattering elements used in EM metamaterials, or transforming EM device designs into acoustic counterparts. One major goal in this field is the fabrication of acoustic cloaks, the theory of which has been discussed by Milton et al. [13], Norris [14], and Norris and Shuvalov [15], to name a few. The realm of acoustic devices that can be enhanced by microstructural design is quite wide. For example, a tunable nonlinear acoustic lens has been fabricated by Spadoni and Daraio [16] and its possible use in biomedical field has been discussed. Control of overall wave propagation using simple microstructure is at the root of all this new development. Here we present experimental support for the possibility of inducing novel phenomena such as tensorial effective density, negative stiffness, density, or negative refraction of stress waves (i.e., anti-parallel phase velocity and group velocity vectors, a sufficient but not necessary condition of which is simultaneous negative effective stiffness and density) using simple microstructures. A

mathematical explanation of such counter-intuitive statements can be found in [17]. An important element in this exposition is to accurately calculate the band structure and dispersion curves of such periodic media in the reciprocal space [1]. This representation may be directly used to derive the group velocity and its relation to the wave vector (phase velocity direction). For example a necessary condition for negative refraction is the negative slope in the dispersion curves relating wave number to frequency. Nemat-Nasser and coworkers [18-20] have developed a general method based on the variational description of the wave equation to calculate band structures of stress waves in arbitrary periodic media. This method has good accuracy and fast convergence. Even though the Nemat-Nasser variational method corresponds to a saddle point in a displacement-only or stress-only variational formulation, it has been proved by Babuska and Osborn [21] that the mixed variational method does converge rapidly to the exact solution. In a more recent paper Milton and Willis [3] present a general framework for such min-max variational principles using Legendre transform. It must be noted here that it is not necessary to use the min-max variational method to derive the band structure. In fact one can use general FEM framework for this kind of calculation. For example, see Phani et al [22] where they model wave propagation in infinite truss lattices using FEM with beam elements.

In this paper, we revisit the method of Nemat-Nasser [18] to calculate the band structure of periodic one-dimensional media. The original work was later on applied to 2D and 3D media by Nemat-Nasser and coworkers [19, 20]. Guided by these calculations, we created laboratory samples of layered media to demonstrate a second pass branch with apparent negative slope within a conveniently measureable frequency range. We show that for this negative branch, the energy-flow direction and phase-velocity direction are opposite to one another, another representation of negative refraction, since the group velocity and energy velocity have the same direction. The transmitted ultrasonic waves were measured for several thicknesses of this layered medium. Through the analysis of the signals, the pass and stop bands were experimentally established and the group and phase velocities were extracted and compared with predicted numerical values. We also calculated a representation of energy velocity by measuring the time for half the pulse energy to travel through each sample. Note that for layered media with each layer having constant properties, the band structure may be calculated exactly, since the wave equation has a closed form solution. The results of the variational method agree with this exact solution with great

accuracy. In 2D and 3D structures, where a closed form solution cannot generally be found, the variational approximate solution is a great alternative since it has high accuracy and fast convergence. Also note that the relationship between the energy velocity and group velocity has been proved by Brillouin and Sommerfeld [23] away from anomalous dispersions. We do not present such a proof for the second branch of layered media here. However, through construction of a pulse consisting of two sinusoidal pulses with a small frequency difference and solving the wave equation exactly, for such disturbance one can simply reveal the anti-parallel nature of phase velocity and group velocity. Furthermore, the energy flux may also be rigorously calculated and it can be shown to have the opposite sign to that of phase velocity in the bands where a negative phase velocity is expected.

2 Calculation of band structure using a mixed variational method

The physical characteristics of wave propagation in periodic media are traditionally represented through polarizations and branches in the band structure graphs, relating normalized wave number $Q = 2\pi(l/\lambda)$(where l and λ represent the unit cell size and wavelength) to the angular frequency ω; see [1, 2] In general for any polarization and wave number there is an infinite spectrum of propagating frequencies.

Consider the stress wave equation

$$\frac{\partial \sigma}{\partial x} = \rho \frac{\partial^2 u}{\partial t^2}, \tag{1}$$

with $\sigma = C\varepsilon$ and $\varepsilon = \partial u/\partial x$ where $u, C(x)$, and $\rho(x)$are the axial stress, strain, displacement, axial stiffness, and mass density, respectively. The 3D exposition can be found in Nemat-Nasser et al [19].

In what follows all physical fields are the real parts of the complex quantities with harmonic time dependence of the form $f_{physical} = Re\left(fe^{-i\omega t}\right)$ The boundary conditions for a unit cell of length l in a periodic medium that supports such waves with the wave number q are,

$$u\left(\frac{l}{2}\right) = u\left(-\frac{l}{2}\right)e^{iql}, \tag{2}$$

$$\sigma\left(\frac{l}{2}\right) = \sigma\left(-\frac{l}{2}\right)e^{iql}, \tag{3}$$

where the origin is at the center of the unit cell. The solutions for waves propagating normal to the plane of a layered medium in 2-phase media is given by Rytov [24]. For approximate evaluation of the eigenvalues one may use the Rayleigh quotient

$$\lambda_R = \omega^2 = \frac{\langle C\partial u/\partial x, \partial u/\partial x\rangle}{\langle \rho u, u\rangle}, \tag{4}$$

where the notation$\langle f, g\rangle = \int_{-l/2}^{l/2} fg^* dx$ with *denoting the complex conjugate, is used. Then the displacement field may be approximated by

$$\bar{u} = \sum_{\alpha=1}^{M} U^\alpha f^\alpha. \tag{5}$$

Here f^α's are linearly independent basis functions and U^α's are the unknown coefficients which are computed by minimizing the Rayleigh quotient. When the stiffness and density are discontinuous the convergence rate of this procedure is very slow due to the discontinuity in the stress fields calculated using continuous base functions. To overcome this difficulty, Nemat-Nasser [18] proposed a new quotient

$$\lambda_N = \frac{\langle \sigma, \partial u/\partial x\rangle + \langle \partial u/\partial x, \sigma\rangle - \langle D\sigma, \sigma\rangle}{\langle \rho u, u\rangle}, \tag{6}$$

based on a mixed variational formulation of the equations of elasticity. Here D is the axial compliance, the inverse of axial stiffness. In this formulation the stress field is approximated independently of the displacement,

$$\bar{\sigma} = \sum_{\alpha=1}^{M} S^\alpha f^\alpha. \tag{7}$$

Minimizing the above quotient, the unknown coefficients, $S^\alpha$and U^α, are obtained from the linear equations

$$\langle \partial\sigma/\partial x + \lambda_N \rho\bar{u},\ f^\alpha\rangle = 0, \tag{8}$$

$$\langle D\bar{\sigma} - \partial\bar{u}/\partial x,\ f^\alpha\rangle = 0. \tag{9}$$

These $2M$ equations can be solved to obtain the unknown coefficients in (5) and (7), and calculate the displacement and stress polarizations (mode shapes). The convergence and efficiency of this method has been established by Babuska and Osborn [21] Furthermore, Nemat-Nasser [18] and recently Nemat-Nasser et al. [25] presented results for simple layered media that show the branch structure calculated through this method matches the exact analytical results with great precision

3 Sample design and numerical predictions

We have measured the phase and group velocities in a layered elastic composite sample consisting of alternating PMMA and steel plates of T_p= 2.95mm and T_s= 0.89mm thicknesses, respectively (to make a symmetric sample, we used PMMA plates of half the thickness $T_p/2$ =1.475mm). The sample is a circular cylinder with D = 16.5mm diameter; see Figure 1. The total

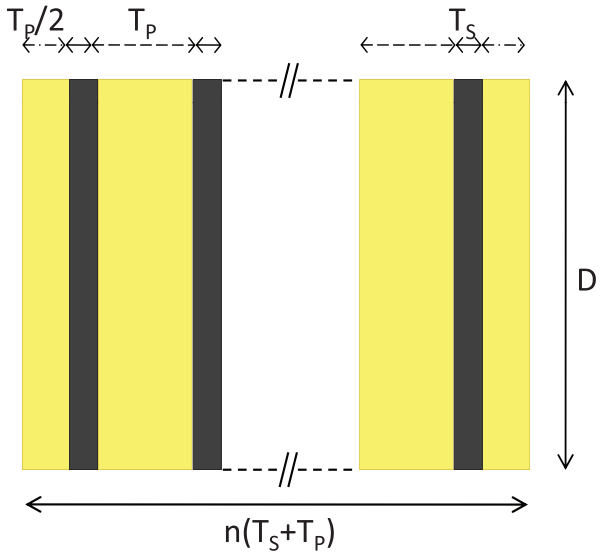

Figure 1: *Sample schematics*

unit cell size l is 3.84mm. The densities of materials were measured to be 1.18g/cc and 7.95g/cc for PMMA and steel, respectively. We also measured the longitudinal wave speed in bare PMMA and steel in the range of frequencies of interest and extracted the corresponding elastic moduli. The resulting longitudinal wave speed values for the bare PMMA and steel are calculated to be 2.7km/s and 5km/s respectively. This results in rather large values of equivalent axial stiffness for PMMA, which is expected in the corresponding high frequency range. Furthermore, because of the high contrast between the elastic moduli of steel and PMMA and small thickness of steel, the static value of the steel's modulus may be used without affecting the final results. Based on these values the band structure for this sample is calculated and is shown in Figure 2.

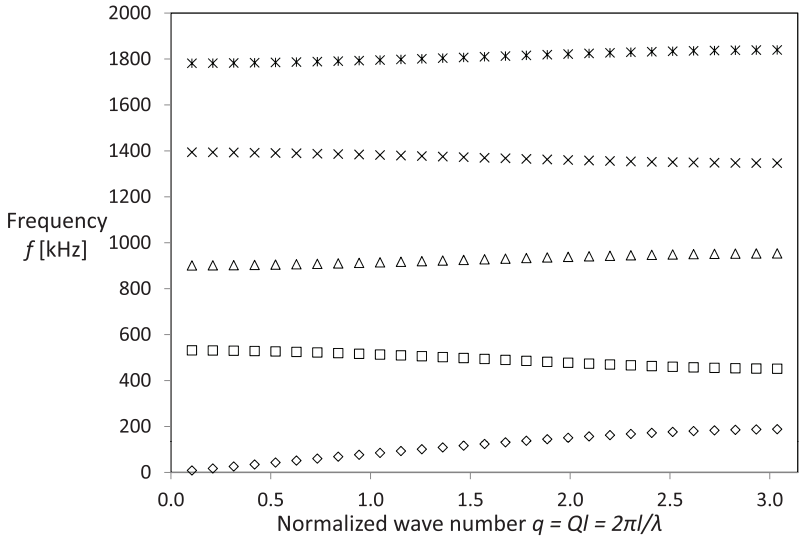

Figure 2: *The dispersion relations and band structures calculated using the mixed variational method.*

4 Experimental measurement of group, energy, and phase velocities

A schematic of the experimental setup is shown in Figure 3. Two Agilent 33220A function/arbitrary waveform generators were used to produce the outgoing signal and trigger which were split and sent to a Tektronix DPO 3014 digital phosphor oscilloscope and to a Ritec GA-2500A gated RF amplifier. A monitor output of amplifier was also sent to the oscilloscope, while the high voltage input was sent to drive a Panametric V103 1MHz longitudinal transducer. The transmitting and receiving transducers (also Panametric V103) as well as the layered sample between them were held together in a transparent plastic cylindrical jacket for proper alignment, and a small axial force was applied to ensure reproducible contact conditions. The surface of the transducers and all the layers were treated with mineral oil to improve transmission and matching of contact surfaces. The output of the receiving transducer was directly sent to the oscilloscope and the corresponding data was collected and stored. The input pulse profile was numerically created and stored in the function generator, to be used with

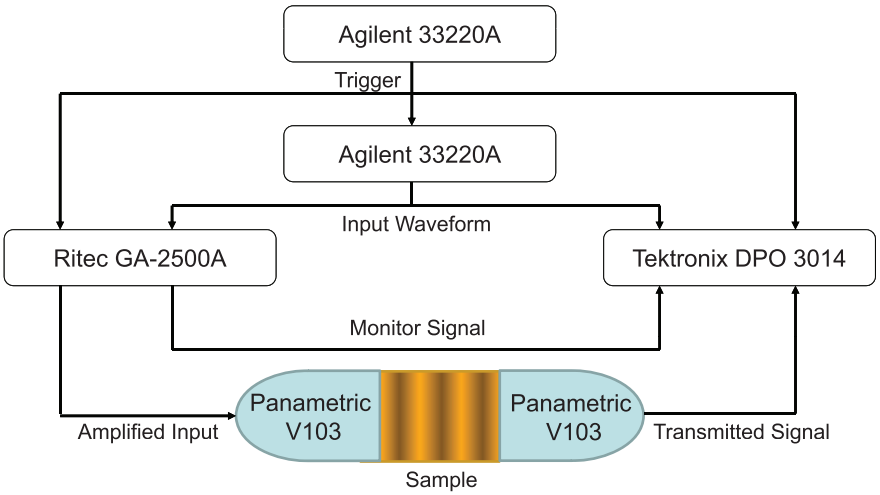

Figure 3: *Schematics of the experimental setup*

various frequencies. The transmitted signals were measured for specimens consisting of n = 3, 4, 5, and 6 unit cells

The driving pulse consists of 10 sinusoidal pulses at the carrier frequency f, multiplied by a half-period of another sinusoidal pulse of 1/20 carrier frequency

$$u\left(0,t\right)=A\sin\left(2\pi ft\right)\sin\left(\frac{2\pi ft}{20}\right)\quad\text{where}\quad 0<t<\frac{10}{f};\tag{10}$$

see Figure 4. The carrier frequency or the total length of the pulse can be changed directly from the function generator. At each frequency step, all three pulses (direct output of function generators, monitor signal of the power amplifier, and received pulse from the transducer) along with the gate step function used to trigger the high-power amplifier were recorded and saved In all cases the measurement started at 50kHz and swept frequencies up to 1.2MHz at 5kHz steps. Two sets of measurements were performed. In

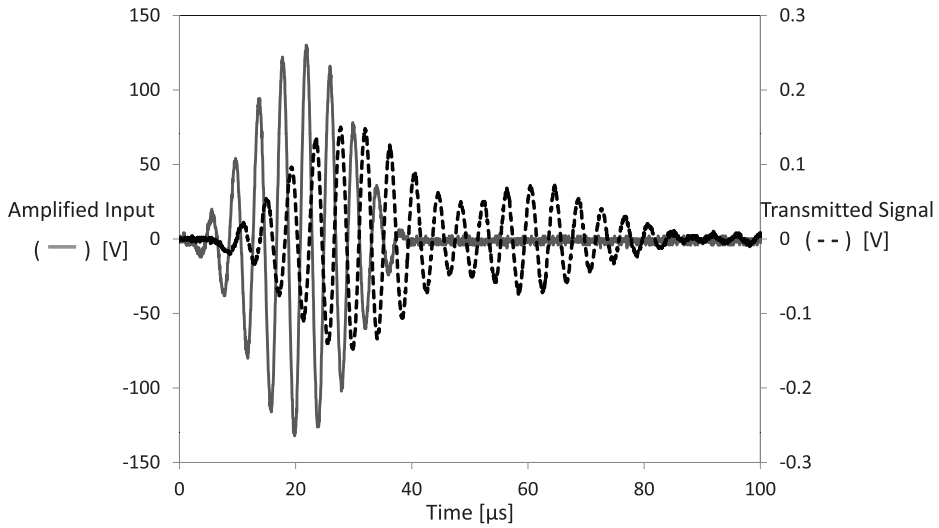

Figure 4: *Input (solid) and transmitted (dashed) pulses*

the first set, the data at each frequency step was stored manually, while in the second set this procedure was automated using a LabView script. Both sets give qualitatively the same results. Minor quantitative differences that were present are discussed below. In general due to the consistency and speedy process of automated data collection, we observed sharper response and cleaner phase measurements compared to the manual procedure.

The collected data were first analyzed in frequency domain. The transmitted amplitudes at the excitation frequency were calculated. The ratio of the transmitted amplitudes at n=3 and n=6 layers is depicted in Figure 5. The first and second stop bands and second and third pass bands can be clearly observed. The low-frequency pass band can also be seen, however the data in this rage are not as clear as for the rest of the spectrum. This can be understood by looking at the absolute power spectra shown in Figure 5 inset. Even when the transducers are directly contacting with no sample in between (at 0 layers), the lowfrequency response is noisy. The transducers geometry and structure are designed for best response around 1MHz. Low frequency (high wavelength) oscillations cannot be studied accurately using such small samples and transducers.

The voltage pulses are sampled at 40ns rate on 10,000 points, digitized

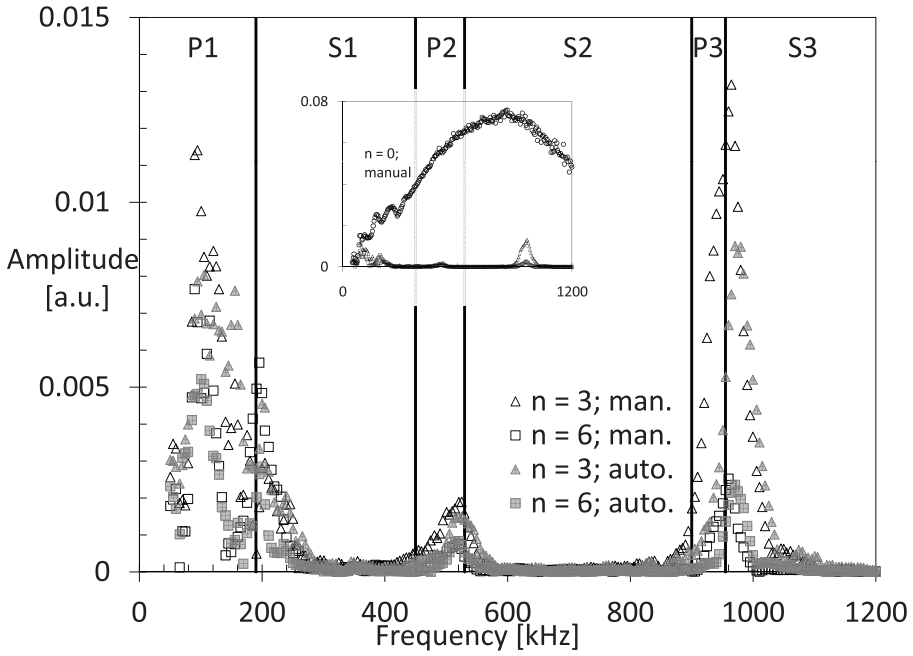

Figure 5: *Amplitude spectrum. Measurements with n = 3 and n = 6 unit cells The data collected manually (man.) and automatically (auto.) are shown with hollow and filled symbols, respectively. The vertical lines show the numerical prediction of the boundaries of first three pass (P1-3) and stop (S1-3) bands. The inset shows the data collected manually when the transducers are put in direct contact with each other (n = 0). The low frequency data (including P1) must be considered in light of the physical limitations of the transducers (e.g. size) and very long wavelengths.*

with 8 bit dynamic range. The oscilloscope has an adjustable amplifier so the absolute range was varied based on the maximum value of the signal to maximize the accuracy of the signal at each frequency value. To minimize noise, a digital filter was applied in the frequency domain, centered at the excitation frequency value. The width of the filter was set at 20% of the central value to ensure that the components of the synthetic input pulse were unaffected. All the frequency components outside this interval were removed. The resulting signal was inverted back to time domain.

The observed pass bands are wider than the calculated ones (less so for the automatically-collected data) and shifted towards higher frequencies

(less so for the manually-collected data). We believe that both these can be attributed to the sample geometry and linear elastic calculation. Simplifications include ignoring the frequency-dependence of the material constituents (non-zero loss and higher modulus at ultrasonic frequencies in the case of PMMA) and geometric dispersion due to finite diameter of samples. In summary the calculated interval for second pass band is 450-535kHz, while the observed bands based on manual and automatic collections are 440-565kHz and 475-575kHz, respectively. These bands agree with phase measurements as explained below in phase velocity calculations.

Group Velocity: In order to calculate the group velocity one measures the time of travel of the pulse as a group for at least two different thicknesses. Due to dispersion the pulse shape changes significantly as it travels through greater number of layers Therefore it is difficult to associate corresponding points to signals that have travelled different distances. We examined two estimation methods. In the first method we find the maximum value of each pulse and use its travel time as the representation of the travel time for the group. In the second method, in addition to the value and time of the peak we find N = 3 other local peaks on either side of the maximum and their amplitudes (a total of 2N+1 = 7 local peaks). A 2N = 6^{th} order polynomial was fitted to these points and the maximum of this polynomial within the interval of the measured peaks was found. We used this maximum and its travel time as the representation for the travel-time of the group (envelope) in this second estimation method The rationale for this approach is that various peaks near the middle of the envelope may have very close measured amplitudes due to dispersion of the pulse. Therefore a small superposed noise may move the estimated absolute maximum from one peak to another neighboring one thus causing an observable difference in the calculated group velocity. The difference between the two methods is small. The second method gives generally smoother results and therefore is presented here. Furthermore, we applied a linear regression fit to the time data from all thicknesses (n = 3, 4, 5, and 6 layers) to calculate the average group velocity. The results are given in Figure 6. One may compare these experimental estimates with the numerical predictions. This shows reasonable agreement within the pass band. Note that the maximum value of the group velocity and its overall shape within the pass bands are the same between prediction and experiment, even though the widths and locations differ slightly. It is not expected that the measured values within stop bands to represent a physical group velocity for a layered medium. The group velocity is obtained

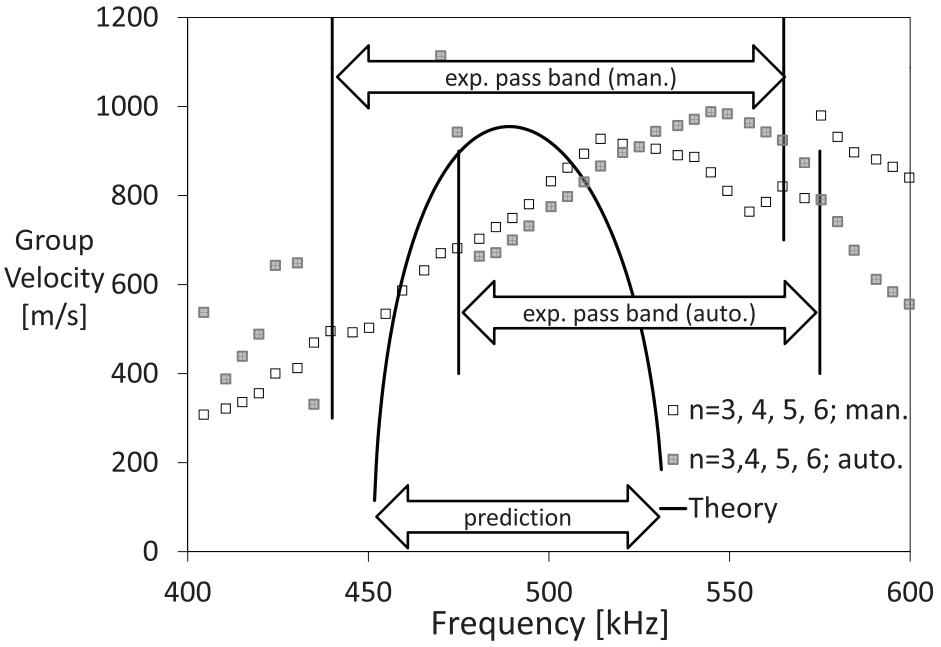

Figure 6: *Group velocity estimations from the experiment and comparison with numerical prediction. The experimental results are based on the second estimation method discussed in this paper and takes advantage of the linear regression of 4 different measurements (n=3, 4, 5, 6 unit cells) data collected manually and automatically. Note that the maximum value of the group velocity and its overall shape within the pass bands are the same between prediction and experiment, even though the widths and locations differ slightly.*

as the slope of the dispersion curve from numerically calculated results,

$$v_g = \frac{\partial \omega}{\partial q}. \tag{11}$$

The wider experimental band and its shift towards higher frequencies are clear here.

Energy Velocity: As an alternative to the group velocity one can measure the energy velocity. It has been shown that the two quantities are equal when dispersion is small [23]. To estimate the energy velocity, we calculate

the total transmitted energy as a function of time, $TE(t)$, as follows:

$$TE\,(t) = F \int_0^t V\,(\tau)^2\, d\tau. \tag{12}$$

Here F is the appropriate conversion factor and $V(t)$ is the measured voltage at time t. The total energy function generally has a trilinear variation as function of time t, consisting of two segments with very small slopes that correspond to the energy content of noise (before and after the stimulation) and a high-slope segment between them representing the bulk of the signal energy. One may use the time at which the value of the transmitted energy reaches half of the total energy for the middle segment of this trilinear function to represent the energy travel-time. Note that there is no need for filtering in this calculation. Similar to the group velocity, the travel-times for 4 experiments with n=3, 4, 5, and 6 unit cells were measured at each excitation frequency. They were then plotted against the sample thickness and linearly fitted. The energy velocity is estimated to be the inverse of the slope of this line. The measured energy velocity for the automatically collected data is shown in Figure 7 and compared with the experimental group velocity. They are in reasonably good agreement within the pass band. The method for estimating the energy velocity is simpler and less sensitive to noise.

Phase Velocity: In order to estimate the phase velocity, the Fourier transform of the signal was calculated. The phase of the Fourier-transform component at the excitation frequency was obtained. The phase difference between thicknesses of n = 3 and 6 unit cells is used in the following discussion since it is less sensitive to noise. However any other two numbers of cells could be used We have focused on the second pass-band where one expects that as the frequency increases, the phase advance through a single unit cell is changed from $Q = \pm\pi$ to $Q = 0$; see Figure 2. The sign is determined to ensure the direction of group velocity is from the transmitter to the receiver. The total phase depends on the number of layers and should be monotonic within a pass band. However the collected data is always within π to π. Therefore through 3 layers, the total phase advance changes from $\pm 3\pi$ to 0. With this in mind one may unfold the phase in the pass band (established based on power measurement) and then shift it by necessary multiple of 2π so that it is closest to zero at the highest frequency of the band. Figure 8 shows the phase difference between measurements of 3 and 6 unit cells and its unfolded counterpart. Dividing by the number of layers, one obtains the

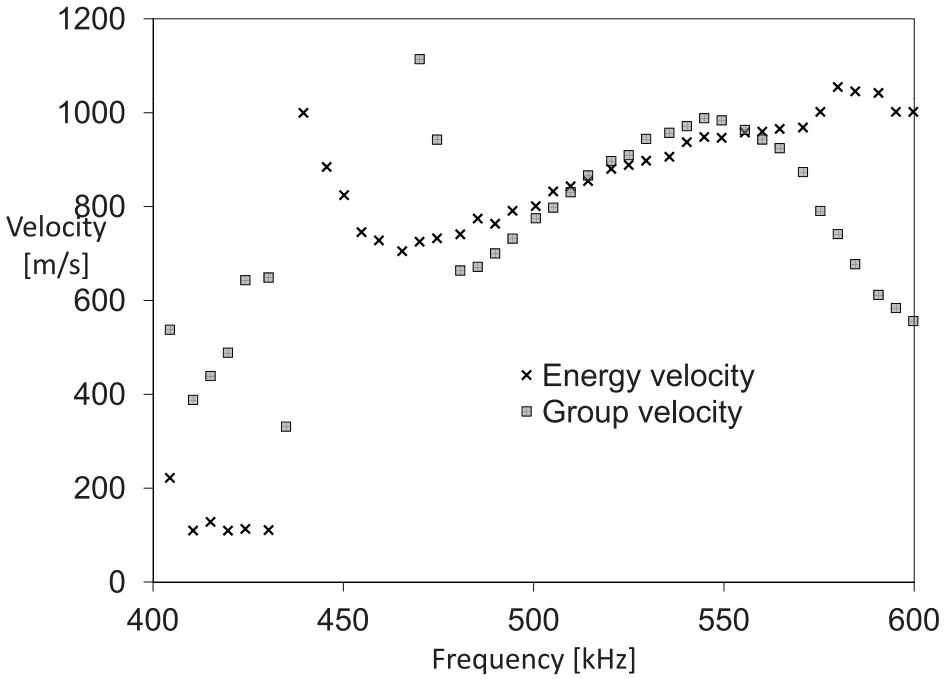

Figure 7: *Energy velocity estimated from linear regression of energy time of travel and comparison with group velocity. The estimated energy velocity agrees well with experimental group velocity within the pass band, while being easier to calculate and cleaner. While the results outside of the experimentally observed pass band are easily calculated, their meaning cannot be attributed to the wave propagation in an infinite medium.*

measured phase difference per unit cell ΔQ, and the phase velocity can now be calculated as

$$v_p = -\frac{\omega}{\Delta Q/l}. \tag{13}$$

The experimental results are shown in Figure 9 and compared with numerical predictions. Note that there is an inherent ambiguity in the amount of shift applied in the process. A number of considerations limit the possible choices. First, within the pass band the absolute value of the phase difference must be reasonably small (for the small number of unit cells considered here). Second, the phase velocity is expected to be continuous within the pass band, therefore the phase difference must not cross zero in this interval. Most other alternatives of the shifting value will give results that are either

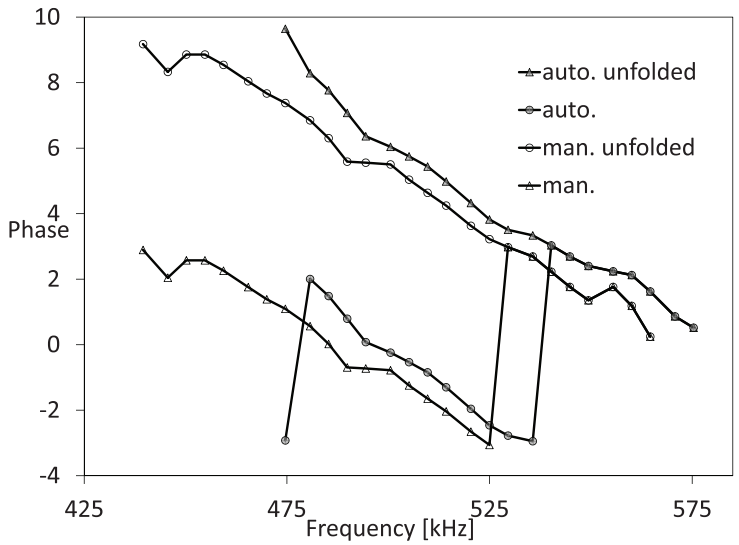

Figure 8: *Measured phase difference between 3 and 6 layers measurements (values within the primary interval $[-\pi, \pi]$) and its continuous unfolding (values within $[0, 3\pi]$) In all cases the data is shown only in the appropriate experimental pass band.*

too small, violating the former requirement, or they may show a singularity within the band, violating the latter. The final condition has to do with the sign of the phase difference. This will be discussed in more detail in the following discussion section. The final selection seems to be unique and agrees with theoretical and numerical predictions.

5 Discussion

The wider transmission bands observed in the experiments can be explained by the dispersive and dissipative nature of PMMA. The material dispersion can be introduced easily in the calculations, and dissipation can also be added with some effort. Another possible factor may be the geometric dispersion due to the finite transverse size of the sample. Due to the sample size and low frequency regime of the experiment this effect is considered of minor importance. It can be taken into account using a dispersive longitudinal wave velocity for each material, essentially combining the material

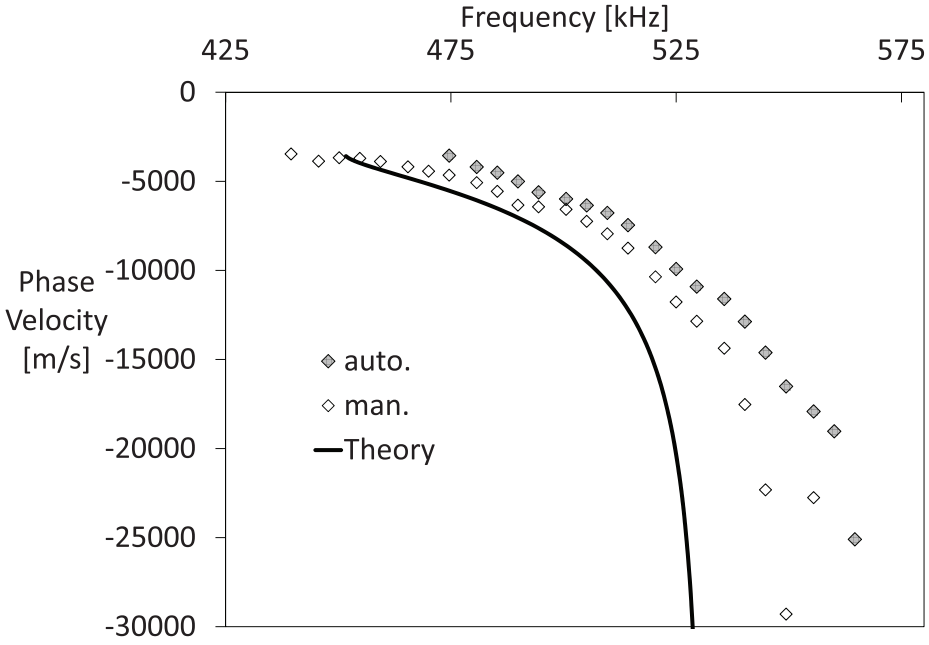

Figure 9: *Experimental phase velocity and comparison with theoretical prediction. The symbols are experimental measurements (manual and automatic collection), while the solid line shows the numerical prediction.*

dispersion and geometric (radial inertia) dispersion. Nevertheless, such expansions are not the subjects of the present paper. Preliminary calculations agree with intuitive expectations that while in a fully elastic medium, the stop bands are absolutely opaque and pass bands are fully transparent, addition of a small dissipation to material properties render the transition between the bands continuous, i.e. the wave travels with large dissipation at frequencies close to the boundaries of the pass bands, while within the stop bands there is very small but nonzero transmission of energy. A thorough analysis of the material loss influence on the acoustic transmission in layered media is subject of further research.

Three requirements were introduced to identify the correct branch for unwrapped phase. The first two, namely continuity of the phase velocity in a pass band (requiring that the phase advance does not change its sign in the interval) and choosing the smallest magnitude of additional $2k\pi$ shift (that

ensures the previous condition) do not need further discussion. However enforcing these conditions gives two possible branches, one fully positive and one fully negative. The choice between the two is made such that the phase velocity becomes negative with respect to the energy transfer. The basis of this negative refraction can be observed by mathematically constructing a group with the dominant frequency in the second (negative) pass band. The envelope travels opposite the single phase components. To visualize this further, one may rigorously calculate the flux at each material cross section of a layered medium using the numerical or analytical solution:

$$EF = \int_0^{2\pi/\omega} -\sigma_{phsyical} v_{physical} dt. \tag{14}$$

This quantity is calculated and shown in Figure 10 as a function of frequency when the phase advance sign is kept always positive. It can be

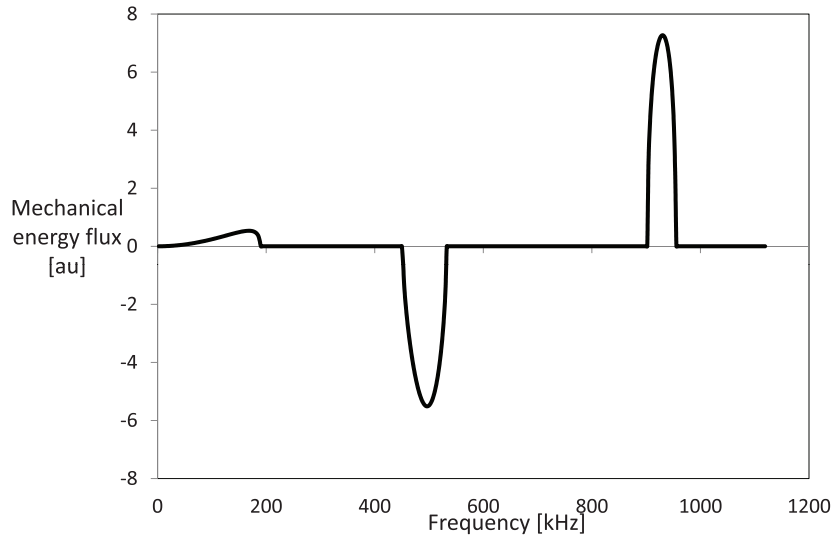

Figure 10: *Energy flux as a function of frequency calculated for a positive phase advance in the principal Brillouin zone, using the theoretical solution of the layered medium.*

clearly seen that within the second (negative) pass band, the energy flux is backward. In the experimental setup, the direction of the energy flux is unchanged, from the transmitter to the receiver. Therefore, the phase velocity will have a negative sign in this branch.

It must finally be noted that the negative phase velocity band discussed above agrees with the pass band observed based on the transmission magnitude. The results for all measured quantities are consistent with a wave vector in the principal Brilloiun zone. For 1D phenomena, there is no further experimental analysis possible. One may study the angular refraction in 2D media similar to Shelby et al. [10] experiment for electromagnetic metamaterials. This is a current subject of research and inherently complex due to the presence of 3 wave modes in solids involving longitudinal and shear stress components. However, Sukhovich et al. [26] have experimentally observed the reversal of Snell's law in a fluid medium through an angular measurement of transmitted power refracted by a wedge. The two-phase microstructure of their sample is the 2D equivalent of the present layered sample. In a solid sample, the presence of shear modes will complicate the experiment and its analysis, but the underlying negative refraction is expected to prevail.

Acknowledgements

The authors wish to thank Jon Isaacs, Robert Kim for making the samples, mechanical and electrical setup of the experiment and collection of data, Ryan Griswold for writing the LabView script for automatic recording of data, and Hossein Sadeghi for automated collection of data. This research has been conducted at the Center of Excellence for Advanced Materials (CEAM) at the University of California, San Diego. This work has been supported by DARPA AFOSR Grant FA9550-09-1-0709 and DARPA U.S. Army RDECOM W91CRB-10-1-0006 grants to the University of California, San Diego.

References

[1] L. Brillouin, Wave Propagation in Periodic Structures; Electric Filters and Crystal Lattices, 2^{nd} ed., Dover, New York, 1953.

[2] C. Kittel, Introduction to Solid State Physics, 7^{th} ed., Wiley, New York, 1996

[3] G. W. Milton and J. R. Willis, Minimum variational principles for time-harmonic waves in a dissipative medium and associated variational principles of Hashin-Shtrikman type, Proc. Roy. Soc. A, 466, (2010) 3013-3032.

[4] J. R. Willis, Effective constitutive relations for waves in composites and metamaterials, Proc. Roy. Soc. A, 467, (2011) 1865-1879.

[5] J. B. Pendry, A. J. Holden, W. J. Stewart, and I. Youngs, Extremely low frequency plasmons in metallic mesostructures, Phys. Rev. Lett., 76, (1996) 4773-4776.

[6] J. B. Pendry, A. J. Holden, D. J. Robbins, and W. J. Stewart, Magnetism from conductors and enhanced nonlinear phenomena, IEEE Transactions on Microwave Theory and Techniques, 47, (1999) 2075-2084.

[7] D. R. Smith, D. C. Vier, W. J. Padilla, S. C. Nemat-Nasser, and S. Schultz, S., Loop-wire medium for investigating plasmons at microwave frequencies, App. Phys. Lett., 75, (1999) 1425-1427.

[8] D. R. Smith, W. J. Padilla, D. C. Vier, S. C. Nemat-Nasser, and S. Schultz, S., A composite medium with simultaneously negative permeability and permittivity, Phys. Rev. Lett., 84, (2000) 4184-4187.

[9] V. G. Veselago, The electrodynamics of substances with simultaneously negative values of ε and μ, Sov. Phys. USPEKHI, 10, (1968) 509.

[10] R. A. Shelby, D. R. Smith, and S. Schultz, Experimental verification of a negative index refraction, Science, 292, (2001), 77-79.

[11] X. Liu, X. Zhang, Y. Mao, Y. Y. Zhu, Z. Yang, C. T. Chan, and P. Sheng, Locally resonant sonic materials, Science, 289, (2000), 1734-1736.

[12] N. Fang, D. Xi, J. Xu, M. Ambati, W. Srituravanich, C. Sun, X. Zhang, Ultrasonic metamaterials with negative modulus, Nature Materials, 5, (2006), 452-456.

[13] G. W. Milton, M. Briane, and J. R. Willis, On cloaking for elasticity and physical equations with a transformation invariant form, New Journal of Physics, 8, (2006), 248, 20 pages.

[14] A. N. Norris, Acoustic cloaking theory, Proc. Roy. Soc. A, 464, (2008), 2411-2434.

[15] A. N. Norris and A. L. Shuvalov, Elastic cloaking theory, Wave Motion, 48, (2011), 525-538.

[16] A. Spadoni and C. Daraio, Generation and control of sound bullets with a nonlinear acoustic lens, Proc. Nat. Acad. Sci., 107, (2010), 7230-7234.

[17] G. W. Milton and J. R. Willis, On modifications of Newton's second law and linear continuum elastodynamics, Proc. Roy. Soc. A, 463, (2007), 855-880.

[18] S. Nemat-Nasser, General variational methods for waves in elastic composites, J. Elasticity, 2, (1972), 73-90.

[19] S. Nemat-Nasser, F. C. L. Fu, and S. Minagawa, Harmonic waves in one-, two-, and three-dimensional composites: Bounds for eigenfrequencies, Int. J. Solids and Structures, 11, (1975), 617-642.

[20] S. Minagawa and S. Nemat-Nasser, Harmonic waves in three-dimensional elastic composites, Int. J. Solids and Structures, 12, (1976), 769-777.

[21] I. Babuska and J. E. Osborn, Numerical treatment of eigenvalue problems for differential equations with discontinuous coefficients, Mathematics of Computation, 32, (1978) 991-1023.

[22] A. S. Phani, J. Woodhouse, and N. A. Fleck, Wave propagation in two-dimensional periodic lattice, J. Acoust. Soc. Am., 119, (2006) 1995-2005.

[23] L. Brillouin, Wave Propagation and Group Velocity, Academic Press, New York, 1960.

[24] S. M. Rytov, Acoustical properties of a thinly layered medium, Sov. Phys. Acoust., 2, (1956), 68-80.

[25] S. Nemat-Nasser, J. R. Willis, A. Srivastava, and A. V. Amirkhizi, Homogenization of periodic elastic composites and locally resonant sonic materials, Phys. Rev. B, 83, (2011), 104103, 8 pages.

[26] A. Sukhovich, L. Jing, and J. H. Page, Negative refraction and focusing of ultrasound in two-dimensional phononic crystals, Phys. Rev. B, 77, (2008) 014301, 9 pages.

Submitted in September 2011

Eksperimentalna potvrda traka naponskih talasa i negativne fazne brzine u slojevitim sredinama

U radu je data analiza i opisana izgradnja slojevitog kompozita, zasnovana na robusnom numeričkom metodu izračunavanja bend strukture naponskih talasa u heterogenim sredinama. Pokazano je da je, na odgovarajucem bend nivou, pravac energetskog toka u dvofaznom kompozitu suprotan faznoj brzini. Obavljena su ekspeimentalna istraživanja prostiranja ultrasoničnih talasa kroz slojevitu strukturu kompozita. Rezultati su uporedjeni sa numeričkim predvidjanjima fazne brzine, grupne brzine, i brzine prostiranja energije, koja su dobijena korisćenjem hibridnog (mjesovitog min-max) varijacionog principa, uz dobru saglasnost. Rezultati numeričkih ispitivanja su takodje u saglasnosti sa egzaktnim resenjima u slučajevima kada se ova mogu dobiti analitičkim putem. Predloženi mješoviti varijacioni metod predstavlja efikasan metod analize prostiranja talasa u slojevitim sredinama.

doi:10.2298/TAM1104299A Math.Subj.Class.: 62K25, 74-05, 74A40,74J99